PERGAMON

International Journal of Heat and Mass Transfer 45 (2002) 4607–4620

International Journal of HEAT and MASS TRANSFER

www.elsevier.com/locate/ijhmt

Dendritic constructal heat exchanger with small-scale crossflows and larger-scales counterflows

Adrian Bejan *

Department of Mechanical Engineering and Materials Science, Duke University, P.O. Box 90300, Durham, NC 27708-0300, USA

Received 8 February 2002; received in revised form 22 April 2002

Abstract

This paper describes the constructal route to the conceptual design of a two-stream heat exchanger with maximal heat transfer rate per unit volume. The flow structure has multiple scales. The smallest (elemental) scale consists of parallel-plates channels the length of which matches the thermal entrance length of the small stream that flows through the channel. This feature has two advantages: it eliminates the longitudinal temperature increase (flow thermal resistance) that would occur in fully developed laminar flow, and it doubles the heat transfer coefficient associated with fully developed laminar flow. The elemental channels of hot fluid are placed in crossflow with elemental channels of cold fluid. The elemental channel pairs are assembled into sequentially larger flow structures (first construct, second construct, etc.), which have the purpose of installing (spreading) the elemental heat transfer as uniformly as possible throughout the heat exchanger volume. At length scales greater than the elemental, the streams of hot and cold fluid are arranged in counterflow. Each stream bathes the heat exchanger volume as two trees joined canopy to canopy. One tree spreads the stream throughout the volume (like a river delta), while the other tree collects the same stream (like a river basin). It is shown that the spacings of the elemental and first-construct channels can be optimized such that the overall pumping power required by the construct is minimal. The paper concludes with a discussion of the advantages of the proposed tree-like (vascularized) heat exchanger structure over the use of parallel small-scale channels with fully developed laminar flow.

Keywords: Constructal design; Tree networks; Dendritic; Heat exchangers; Modules; Topology optimization; Hierarchical design

1. Constructal theory and design

The subject of this paper is the constructal architecture that gives a heat exchanger the ability to pack maximum heat transfer rate in a fixed volume. The constructal method of optimizing flow architectures has been applied in several areas: the method and its published applications are reviewed in [1]. The application described in the present paper is new. It reveals the modular, hierarchical architecture with the most dense heat transfer packing for one of the most frequently used thermal engineering devices—the heat exchanger. This application is considerably more general, because the maximization of heat transfer density per unit volume is key to the development of microscale heat transfer devices in many sectors of engineering [2–6].

Constructal theory and design is a hierarchical way of thinking that accounts for organization, complexity and diversity in nature, engineering and management [1]. It was first stated in 1996, in the context of optimizing the access to flow between a point and an area, with application to traffic [7] and the cooling of electronics [8]. The flow path was constructed in an "atomistic" sequence of steps that started with the smallest building block (elemental area) and continued in time with larger building blocks (assemblies or constructs). The mode of transport with the highest resistivity (slow flow, diffusion, walking, and high cost) was placed at the smallest

* Tel.: +1-919-660-5309; fax: +1-919-660-8963.
E-mail address: dalford@duke.edu (A. Bejan).

0017-9310/02/$ - see front matter
PII: S0017-9310(02)00165-5

Nomenclature

a	group (m^2), Eq. (11)
$c_1, \ldots, c_4$	constants of integration
D_c	cold-side channel spacing (m), Fig. 11
D_h	hot-side channel spacing (m), Fig. 11
D_h	hydraulic diameter (m)
D_0	elemental spacing (m)
D_1	side-jacket spacing (m), Fig. 3
K	permeability of parallel-plates channels (m^2)
L	length (m)
$\dot{m}$	mass flow rate (kg/s)
n_1	number of elemental volumes in the first construct
n_2	number of first constructs in the second construct
P	pressure (Pa)
Pr	Prandtl number
R_0	rib spacing (m), Fig. 1
S	area (m^2)
U, U_0	mean velocities (m/s)
V	volume (m^3)
W_0	elemental width (m), Fig. 11
x	dimensionless group, Eq. (20)
X_T	thermal entrance length (m)
z	height (m), Fig. 11

Greek symbols

α, β, γ	layers, Fig. 7
μ	viscosity (kg/s m)
ν	kinematic viscosity (m^2/s)
ρ	density (kg/m^3)

Subscripts

c	cold
end	closed end
h	hot
in	inlet
min	minimal
out	outlet
0	elemental volume
1	first construct
2	second construct

scales, filling completely the smallest elements. Modes of transport with successively lower resistivities (fast flow, streams, vehicles, and low cost) were placed in the larger constructs, where their purpose was to connect the area-point or volume-point flows integrated over the volume. The geometry of each building block was optimized for area-point or volume-point access, i.e., for minimum global flow resistance. The architecture that emerged was a tree in which every geometric detail is a result—the tree, as a geometric form *deduced* from a principle.

For simplicity, in this paper I consider the heat exchanger between two streams with the same capacity rate, Fig. 1. Each stream carries a single-phase fluid (e.g., gas, or liquid) with constant properties and a Prandtl number of order 1 or greater than 1. More general (unbalanced) heat exchangers for single-phase and/or two-phase flow can be configured by using the method described here (e.g., Section 6).

2. Elemental volume: smallest size, fixed

In the simplest description, every flow passage can be modeled as a two-dimensional space formed between two parallel plates. Two such passages are shown in counterflow in Fig. 1a, and in crossflow in Fig. 1b. A sandwich of only two passages is called *elemental volume*, and is labeled (0). The elemental volume is the geometric feature with the smallest scale in the considerably larger and more complex structure that is the heat exchanger. The smallest scale is fixed (see also Section 7). The envisioned structure contains a large number of elemental volumes, which are arranged in vertical stacks indicated with dashed lines in Fig. 1b. The challenge is to find the flow architecture, i.e., the best way to connect and assemble the elemental volumes into a much larger device that receives and discharges only two streams, one hot and the other cold. The challenge is to bathe the entire volume with the two streams, and, later, to reconstitute the streams before they are discharged.

The proposed architecture has several new features, and several old ones. An old feature is the crossflow arrangement chosen for each elemental volume (Fig. 1b). It is known that the best arrangement from a thermodynamic optimization point of view is the counterflow: in the counterflow configuration, the entropy generation rate for a fixed heat transfer area is the smallest, and vanishes when the area increases to infinity [9]. The need to stack many elemental volumes together makes the use of counterflows at the smallest scales difficult, if not impossible. This is especially true when the passage dimension (the spacing between plates) is small. It is difficult to distribute many streams of type 1 from one side of the assembly, while having to collect many streams of type 3 on the same side of the assembly.

This difficulty is eliminated by the crossflow arrangement, where each of the four sides of the assembly of elemental volumes is devoted to distributing or collecting a single stream that flows through many elemental slits in parallel. Counterflows are not abandoned,

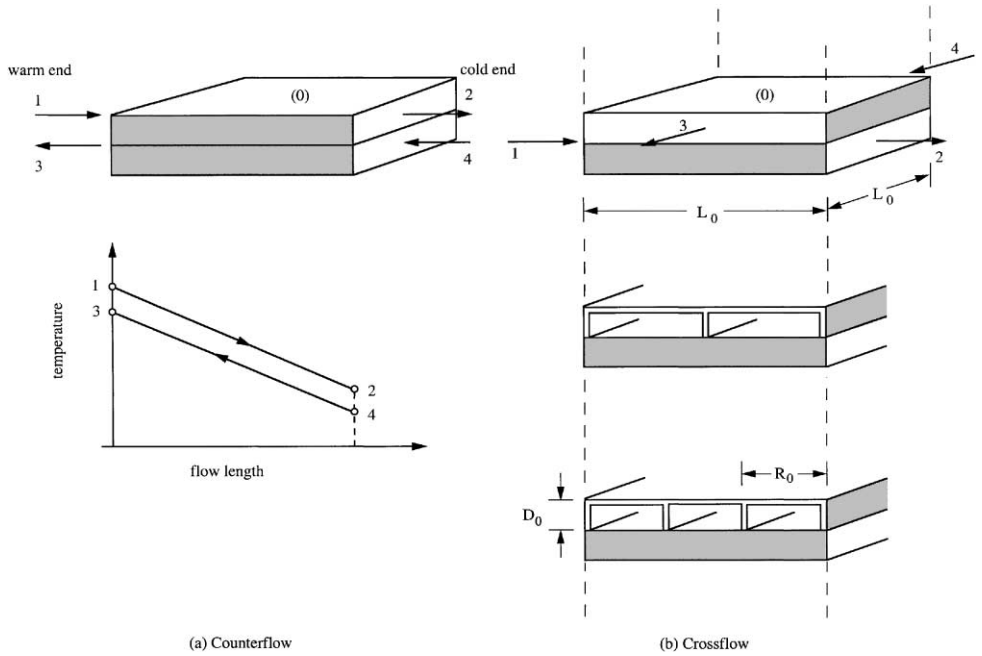

Fig. 1. Elemental volumes containing two flow passages: (a) counterflow and (b) crossflow.

however. They are used in all the subsequent (larger) scales of construction (the first construct, the second construct, etc.), where the use of counterflows is not as difficult as at the elemental level.

Another old feature is the solid material into which the flow structure is machined. The material must be one with high thermal conductivity, e.g., aluminum, or silicon. The outer surfaces of the entire heat exchanger are insulated with respect to the ambient.

One new feature is that most of the heat transfer between the two streams occurs in the elemental volumes, across small separating surfaces of type $S = L_0 \times L_0$, as shown in Fig. 1. The two streams will come in contact by counterflow at larger scales, in the larger ducts that distribute the streams to (and later collect the streams from) the elemental volumes. The following labeling convention is used for the four ports of a volume, regardless of the size of the volume:

1. the inlet of the warm stream,
2. the outlet of the warm stream,
3. the outlet of the cold stream,
4. the inlet of the cold stream.

Taken together, ports 1 and 3 constitute the "warm side" of the volume. Ports 2 and 4 constitute the "cold side".

The key feature is that the dimensions of every flow passage are such that the flow is laminar, and the flow length matches the thermal entrance length, $L_0 \cong X_T$. The reason for selecting this feature is explained in Refs. [10,11] and Fig. 2. Let D_0 and U_0 be the plate-to-plate spacing and mean velocity of one elemental passage. The entrance is the region where thermal boundary layers are present. The thermal entrance length X_T is the approximate longitudinal position where the thermal boundary layers have just merged. Downstream of X_T, the temperature distribution across the channel has a fully developed profile. Said another way, the stream must travel a certain distance (X_T) before it is penetrated fully by the diffusion of heat from or to the wall. Although the value of X_T is not a precise number, its order of magnitude is certain and valid for all Pr values, $Pr > 1$ and $Pr < 1$ (e.g., Ref. [11, pp 122–132]),

$$\left(\frac{X_T/D_h}{Re_{D_h}Pr}\right)^{1/2} \cong 0.2 \tag{1}$$

where $Re_{D_h} = U_0 D_h/\nu$, with ν as the kinematic viscosity of the fluid, and D_h as the hydraulic diameter, $D_h = 2D_0$. Selecting the elemental flow length such that $L_0 \cong X_T$, we find from Eq. (1) that

$$\frac{L_0}{D_0} \cong (0.16)\frac{U_0 D_0}{\nu} Pr > 1 \tag{2}$$

If D_0 is the smallest dimension that can be manufactured, then L_0 is dictated by Eq. (2) when U_0 is known.

The elemental velocity U_0 is known as soon as the volume and macroscopic streams of the entire heat exchanges are specified. Let V and $\dot{m}_h$ be the total volume

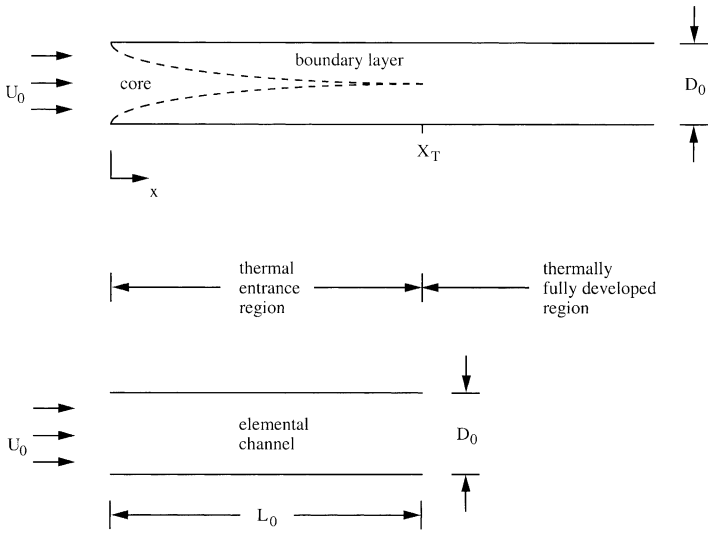

Fig. 2. The flow length of the elemental channel (L_0) must match the thermal entrance length of the laminar flow (X_T).

and the mass flow rate of the hot streams that must be distributed throughout V. According to the constructal method (Sections 3–5) the volume V is filled by interconnected elemental volumes. The order of magnitude of the cross-sectional area of V is $V^{2/3}$. The stream $\dot{m}_h$ perfuses with the velocity U_0 through the $V^{2/3}$ area, therefore, from mass conservation, $U_0 \approx \dot{m}_h/(\rho V^{2/3})$.

Here is the reason for choosing an elemental length that matches the thermal entrance length. The key to packing maximum heat transfer per unit volume is the observation that every infinitesimal packet of fluid must be used for the purpose of transferring heat. Fluid flow regions that do not work must be avoided. Flow regions that worked too much, and are now ineffective, must be eliminated.

With reference to the top drawing of Fig. 2, the designer has two choices, and both are not the best. If L_0 is made shorter than X_T, then the fluid that occupies the core of the duct does not participate in the heat transfer enterprise. Such fluid must not be allowed to leave the elemental channel without having interacted thermally with the walls. In the other extreme, when L_0 is made longer than X_T, all the fluid has interacted with the walls. This fluid is so saturated with heating or cooling from the wall, that it can accommodate further heating or cooling only by overheating, i.e., by changing its bulk temperature in the downstream direction. This extreme (the fully developed regime) must be eliminated. It is important to note that the decision to avoid the thermally fully developed flow regime contradicts current trends in microscale heat exchanger, where laminar fully developed flow is seen as the key to maximizing the heat transfer density. We return to this important difference in Section 7.

The best choice is in-between, $L_0 \approx X_T$, because in this configuration all the fluid of the channel cross-section "works" in a heat transfer sense. The fluid leaves the channel as soon as it completes its mission. In this configuration the elemental volume is used to the maximum for the purpose of transferring heat between the stream and the walls.

The elemental channel may have a variety of cross-sectional shapes that are represented by the spacing D_0. Several designs are sketched in Fig. 1b. The elemental duct of cross-section $D_0 \times L_0$ could be a bundle of parallel channels machined or etched into high-conductivity wall material. The ribs between the machined channels serve as fins, and provide mechanical strength for the elemental assembly. The ribs are not new features. New is the idea that if the spacing between ribs is R_0, and if D_0 is smaller than or equal to R_0, then the elemental duct $D_0 \times L_0$ must be designed in accordance with Eq. (2). The important dimension of the smallest cross-section ($D_0 \times R_0$) is the smaller of the two dimensions, namely D_0. The elemental volume geometry must be optimized by selecting L_0, D_0 and U_0, such that Eq. (2) is respected as closely as possible. This holds for both sides of the heat transfer surface S, and, consequently, the elemental surface S must be a square of side L_0.

3. First construct: assembly of elemental volumes

A large number (n_1) of elemental volumes can be assembled into a larger system, in the manner shown in Fig. 3. This larger system is called a *first construct* [1]. It is a parallelepiped of size $L_1 \times L_0 \times L_0$, where, if the solid elemental walls are thin in comparison with D_0, then

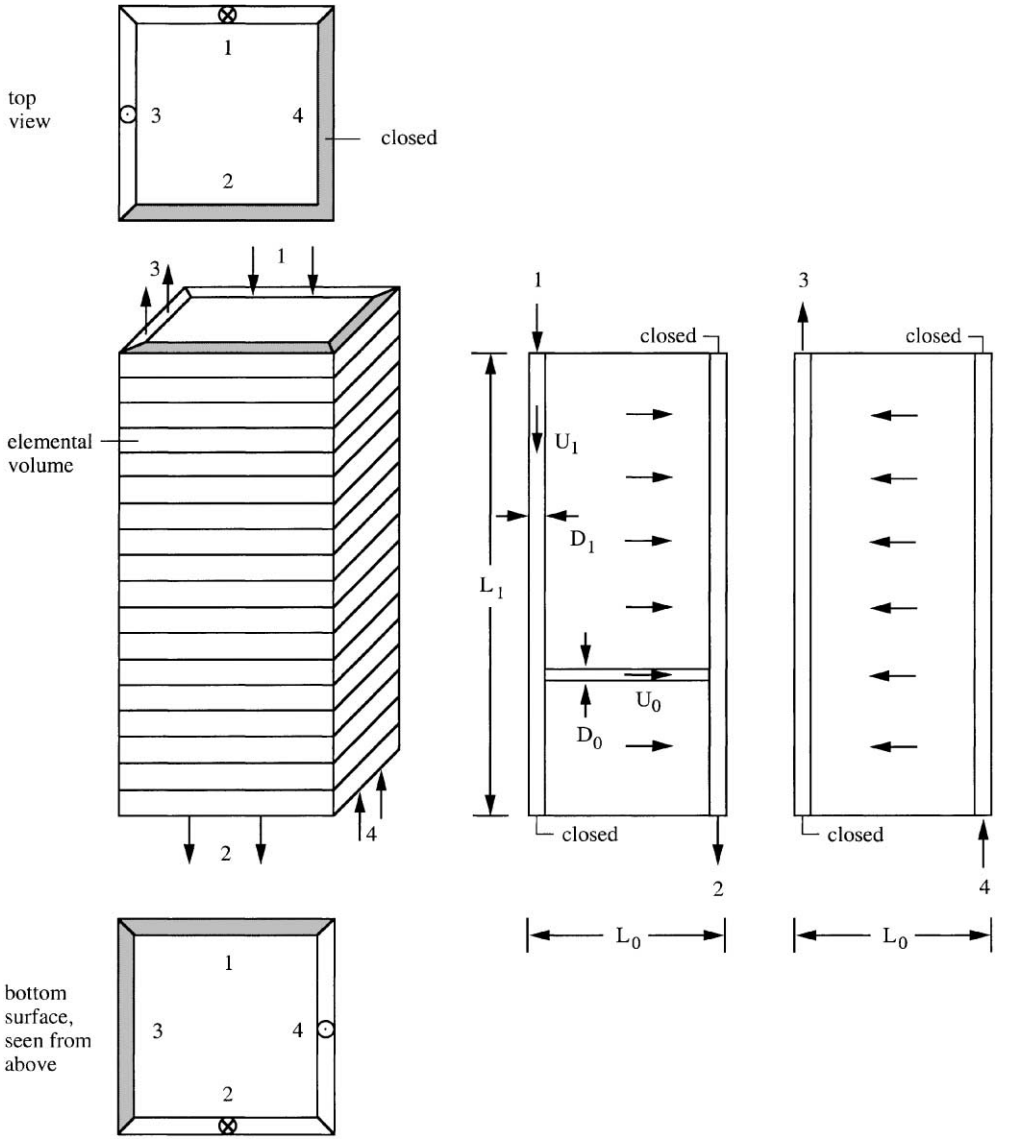

Fig. 3. First construct containing a large number of elemental volumes (Fig. 1) stacked in the D_0 direction.

$L_1 = 2n_1D_0$. This assembly has a fluid jacket of height L_1 and spacing D_1. The jacket is divided into four vertical parallel-plate channels of cross-section $D_1 \times L_0$, one channel for each side of the $L_0 \times L_0$ square base. Each $D_1 \times L_0$ channel is closed at one end. The cross-section of the $D_1 \times L_0$ channel may have ribs for mechanical stability and additional heat transfer (e.g., Fig. 1b), but such details are not essential as long as D_1 is the smaller dimension of the $D_1 \times L_0$ cross-section (see the discussion that ended Section 2).

The streams enter and exit the first construct through slits: two slits at the warm end of the construct, and two at the cold end. These ports are paired together such that one end of the stack becomes the warm side, and the other end becomes the cold side. Seen from the outside, the first construct resembles the counterflow arrangement shown in Fig. 1a. This is an important step in the construction. The first construct is the first module (the smallest scale) where the crossflows of the elemental volumes are organized in such a way that they give birth to counterflows of a larger scale.

Stream 1 enters vertically through a D_1-wide slit, flows horizontally through the stack of n_1 elemental channels of spacing D_0, and continues vertically through another D_1 channel to exit no. 2. The cold stream follows a similar path, as shown on the right side of Fig. 3.

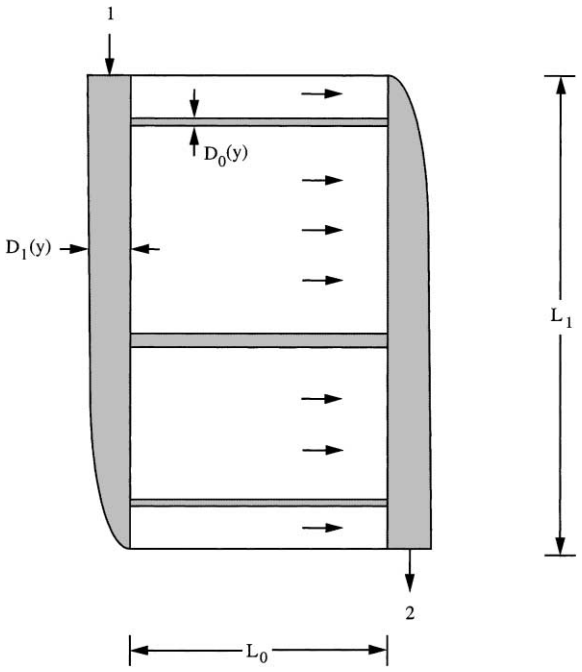

Fig. 4. First construct with variable D_1 and D_0, and uniform flow through the stack of elemental volumes.

In this simplest description of the first construct, the jacket spacing D_1 and the elemental spacing D_0 were assumed constant. In such a design the horizontal flow through the elements that form the core of the first construct would be distributed nonuniformly. Specifically, the velocity U_0 through the top and bottom regions of the stack would be larger than through the mid-height regions. This flow can be made uniform by using (a) tapered D_1 channels that reach $D_1 = 0$ at their closed ends, and (b) smaller D_0 spacings in the top and bottom portions of the stack. See Fig. 4. Past experience with the optimal tapering of channels and fins shows that, if implemented, such structural details can improve the overall performance by changes of the order of 10 – and D_0. We focus more closely on the design of the first construct in Section 6.

4. Second construct: assembly of first constructs

The assembly of a number (n_2) of first constructs is called *second construct*. An example with $n_2 = 5 \times 5$ is illustrated in Fig. 5. The key to this arrangement is the counterflows formed between streams 1 and 3, and 2 and 4. In other words, when two of the first constructs shown in Fig. 3 are fused together, their lateral surfaces of size $L_1 \times L_0$ are fused in such a way that the surface with outlet no. 3 is fused with the surface with inlet no. 1. Similarly, the surface with the cold inlet no. 4 is fused with the no. 2 surface of another first construct. This construction is illustrated in Fig. 6.

The second construct is a parallelepiped of height L_1 and base $n_2 L_0^2$. The base is not necessarily square. If the total volume allotted to the second construct is V_2, and if the shape of the V_2 parallelepiped is also specified, then several internal architectural features $(n_1, n_2, \ldots)$ can be selected such that the size and shape of the second construct match the size and shape of the available space.

Fig. 5b shows how the top side of the second construct looks when it is viewed from above. The top surface is pierced by counterflows of fluid sheets 1 and 3. Fig. 5c shows the corresponding view of the bottom side, when the bottom side is also viewed from above. Note the vertical alignment of corners A and A′, B and B′, etc. The bottom surface is pierced by counterflows of fluid sheets 2 and 4.

The top and bottom end plates have the purpose of reorganizing the streams. They connect all the fluid sheets of one type (e.g., sheet 1, Fig. 5b) to a single inlet or outlet that supplies or discharges the stream of that type. Another feature is that the flow network that connects all the streams of type 1 is placed in balanced counterflow with the flow network that connects all the streams of type 3. Similarly, at the bottom end of the second construct, the flow network that connects the streams of type 2 is placed in balanced counterflow with the network connecting the streams of type 4. Tree-shaped flows in balanced counterflow are a prevailing flow structure in sub-skin vascularized tissues [12,13]. The purpose of the intimate thermal contact between the streams in counterflow is to minimize the leakage of heat (an enthalpy current) along the counterflow, from the warm end to the cold end. The counterflow provides thermal insulation in the flow direction: this insulation effect has its origin in the minimization of thermal resistance in the direction perpendicular to the streams (e.g., Ref. [9, p. 522]). This special feature, and the fact that the streamwise leakage of heat vanishes as the thermal contact between streams becomes perfect, is the reason why the balanced counterflow is the best arrangement from the point of view of minimizing heat transfer irreversibilities.

Each of the four networks connects one point (source, or sink) to n_2 points distributed almost uniformly over the top or bottom areas. The n_2 "points" are thin slits of size $D_1 \times L_0$. There are several flow structures that effect such point-area connections. The most effective are the tree-shaped networks [1]. One example is shown in Fig. 7: note the superposition of two tree-shaped flows in counterflow, namely, streams 2 and 4.

The two trees are machined into the plate that caps one end of the second construct. Let us focus on the bottom end, A′B′C′D′. The end plate is a sandwich of three layers (α, β, γ). The inner layer (α) makes contact

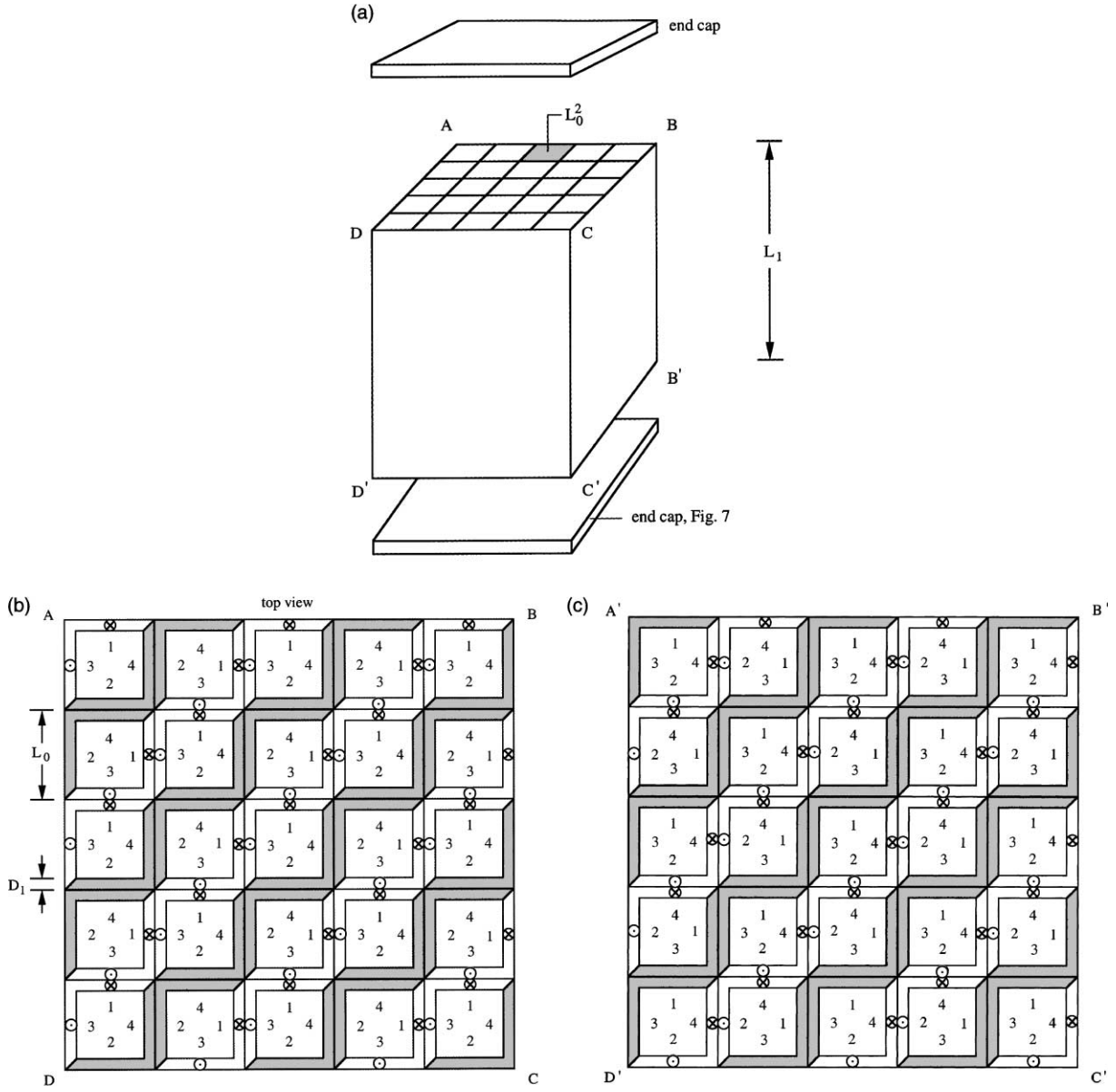

Fig. 5. Second construct containing a number of first constructs.

with the $A'B'C'D'$ surface, and has parallel rows of perforations that communicate with the slits of type 2 and 4 of the $A'B'C'D'$ surface. Rows that communicate with slits of type 2 alternate with rows that communicate with slits of type 4. The traces of these perforations are indicated with dots and crosses on the $A'B'C'D'$ frame shown in Fig. 7. The rows are parallel to the diagonal of the $A'B'C'D'$ square. On the outer side of layer α, the orifices communicate with channels that collect the fluid of only one type (e.g., type 2), and separate it from the fluid of the competing type (e.g., type 4).

The next layer (β) caps the α channels. Layer β has only two rows of orifices, which connect all the α channels of one type, and place their fluid in counterflow with the fluid of the second type. The orifices of the two channels of layer β are projected on the plane $A'B'C'D'$ in Fig. 8a. The α and β channels of the same fluid type are arranged in a dendritic pattern, where the branches (or tributaries) are perpendicular to the stem. See the three-dimensional representation of this configuration, Fig. 8b. Dendritic patterns of other types can be machined into the α and β layers.

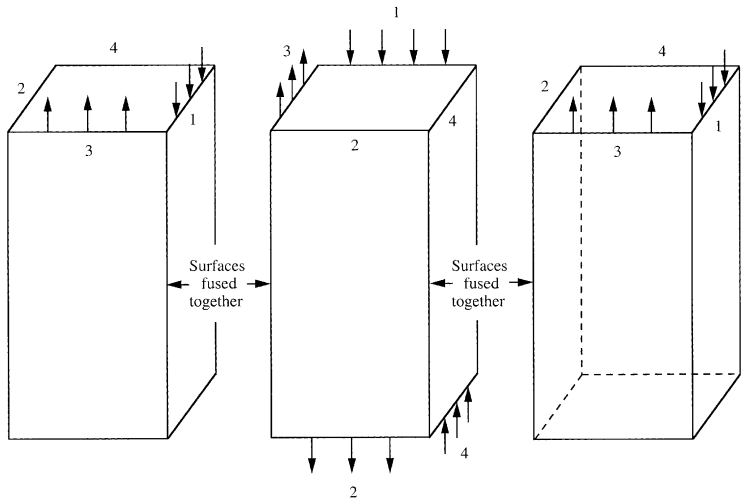

Fig. 6. The formation of counterflows during the assembling of the second construct shown in Fig. 5.

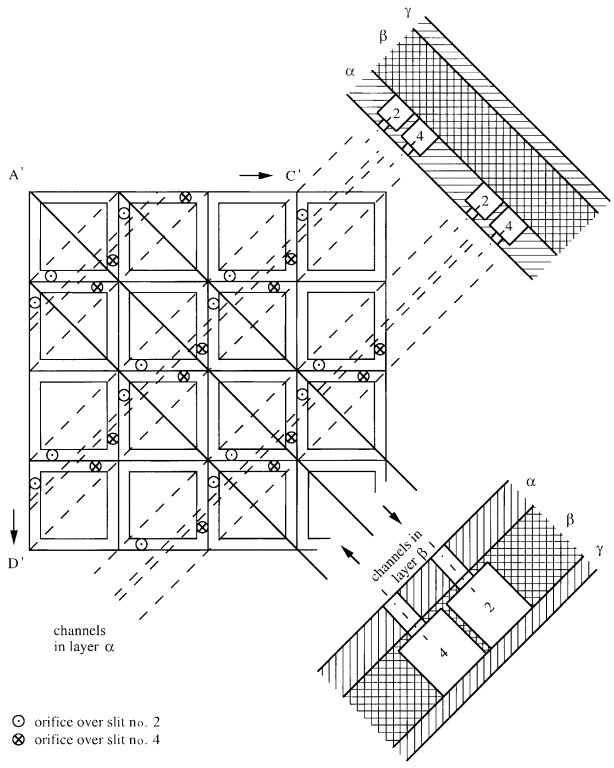

Fig. 7. The construction of counterflow tree-shaped networks in the α and β layers of the second-construct end plates.

The function of layer γ is to cap the β channels. One of the two ports machined into the γ layer allows the total stream of type 2 to leave the second construct. The other port is the inlet of the total stream of fluid 4.

In summary, the second construct is an arrangement that unites the large number of mini-streams of fluid, and delivers to the outside just two outflowing macroscopic streams (2 and 3). At the same time, the architecture of the second construct allows the two inflowing

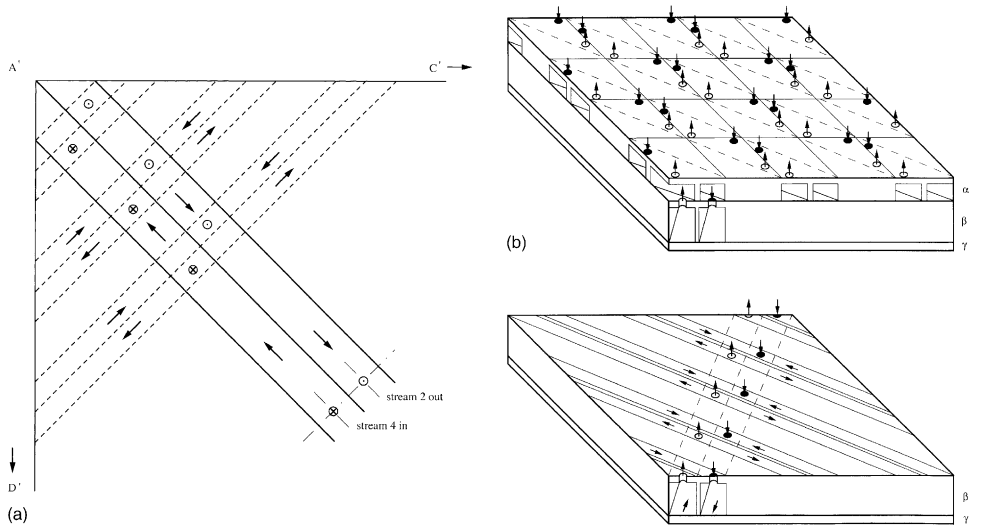

Fig. 8. (a) The connections between the α and β channels, and the two ports (inlet, outlet) of the cold end of the second construct. (b) Three-dimensional representation of the construct of Fig. 7.

streams (1 and 4) to spread through the entire volume, and bathe every single elemental volume in practically the same way (see Fig. 2). At scales of construction that are larger than those of the elemental volume, every stream and flow channel is placed in counterflow with a stream and channel of the same size. These counterflows force the two macroscopic streams to exchange heat at every scale, all the way to the largest scale. Note the counterflow formed between the two channels of the β layer. By making these channels relatively deep, we can maximize the thermal contact between the two streams.

5. Third construct: assembly of second constructs

In the construction example of Figs. 5–8, the integrated streams (1, 2, 3, 4) enter and exit through the centers of the two end caps of the second construct. This example, Fig. 9a, was chosen only for illustration because it maximizes symmetry inside the construct.

It is not necessary to place the inlet–outlet pairs in the centers of the end caps. The trees of channels dug into the α and β layers could be configured in such a way that the 1–3 and 2–4 pairs are positioned anywhere on the top and bottom surfaces of the construct. For example, the inlet–outlet pairs can be placed in one of the four corners, as shown in Fig. 9b. This degree of freedom is important, especially when the volume made available for heat exchange is larger than that of one second construct. Fig. 9c shows how four second constructs can be clustered into a *third construct*, which is supplied by two streams (1 and 4), and which discharges only two streams (2 and 3). This third construct is formed by arranging four of the second constructs of Fig. 9b in such a way that they share the generator connecting the $(1,3)$ corner with the $(2,4)$ corner. The top side of Fig. 9c is the warm end of the counterflow, and the bottom side is the cold end.

Larger third constructs can be made by assembling more than four second constructs. In every case, the rule is to guide streams 1 and 3 in counterflow into the third construct, and into the second constructs that are present in the third construct. Fig. 10 shows how to assemble a large number of second constructs (Fig. 9a) or third constructs (Fig. 9c), into a much larger volume. Streams 1 and 3 form one counterflow tree that invades the interstices of a second counterflow tree, which is formed by streams 2 and 4. The two intertwining trees of Fig. 10 are drawn in two dimensions for the sake of simplicity. Similar two-tree structures, in which each tree is a counterflow of two streams, can be constructed in the three-dimensional space. Either in two dimensions or three dimensions, the largest volume (the macroscopic system) has a pair of mating ports $(1,3)$ at its warm end, and another pair $(2,4)$ at its cold end.

6. Geometric minimization of flow resistance

In this section we illustrate how some of the geometric features of the flow architecture can be optimized by minimizing the global resistance to fluid flow through the structure. Consider the flow through the first construct (Fig. 3), and assume the more general case where the capacity rates are not balanced. Fig. 11 shows that instead of the $L_0 \times L_0$ notation for the dimensions of the

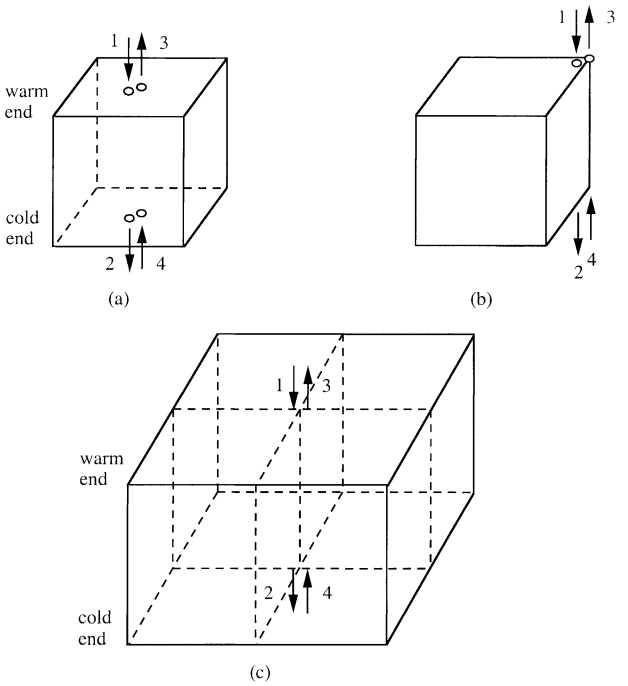

Fig. 9. (a,b) The freedom to position the inlet–outlet pairs in the end caps of a second construct. (c) The formation of a third construct by clustering four second constructs.

elemental heat transfer surface, we use $L_0 \times W_0$, where in general $L_0 \neq W_0$. Instead of the vertical channel spacing D_1, we use D_c and D_h. The subscripts c and h indicate the cold and hot streams, respectively. The two streams follow the paths 1–2 and 4–3: we analyze in detail only the flow path 1–2, because the optimization results for the path 4–3 can be deduced later by inspection.

The path 1–2 consists of two vertical parallel plate channels of spacing D_h, which are connected through a porous core (0) of horizontal permeability K_{0h}. The treatment of the stack of elemental channels as a porous medium with Darcy-like flow is justified, because when each channel functions as shown in Fig. 2, the pressure drop along the channel is of the same order of magnitude as in fully developed flow. The permeability K_{0h} is shorthand for $D_{0h}^2/12$, in accordance with the porous medium characterization of a stack of parallel fissures (e.g., Ref. [11, Problem 12.3]). The use of the porous medium description at the elemental scale is justified because of the never-ending march toward small scales in complex designs. In this direction, constructal flow architectures become *designed porous media*.

The hot stream $\dot{m}_h$ enters through the upper-left corner of the $L_0 \times L_1$ rectangle, and exits through the lower-right corner. We are interested in minimizing the pressure drop between these two corners. The following analysis is based on the observation that the flow distribution is symmetric about the center of the $L_0 \times L_1$ rectangle. Consequently, we set $z = 0$ at mid-height, and recognize that the flow rates may vary along the left-side channel, $\dot{m}_1(z)$, and along the right-side channel, $\dot{m}_2(z)$. The end values of these flow rates are known

$$\dot{m}_1(L_1/2) = \dot{m}_2(-L_1/2) = \dot{m}_h \tag{3}$$

$$\dot{m}_1(-L_1/2) = \dot{m}_2(L_1/2) = 0 \tag{4}$$

Mass conservation requires $\dot{m}_1 + \dot{m}_2 = \dot{m}_h$ at any z, or

$$d\dot{m}_1 = -d\dot{m}_2 \tag{5}$$

The horizontal flow rate through the K_{0h} core is

$$d\dot{m}_1 = \rho u W \, dz \tag{6}$$

where u is the volume averaged velocity. Because the core behaves as a porous medium with Darcy flow, we write

$$u = \frac{K_{0h}}{\mu L_0}[P_1(z) - P_2(z)] \tag{7}$$

The pressure distributions along the side channels (P_1, P_2) are related to the flow rate distributions $(\dot{m}_1, \dot{m}_2)$,

$$\dot{m}_1 = \rho D_h W_0 \frac{K_h}{\mu} \frac{dP_1}{dz} \tag{8}$$

$$\dot{m}_2 = \rho D_h W_0 \frac{K_h}{\mu} \frac{dP_2}{dz} \tag{9}$$

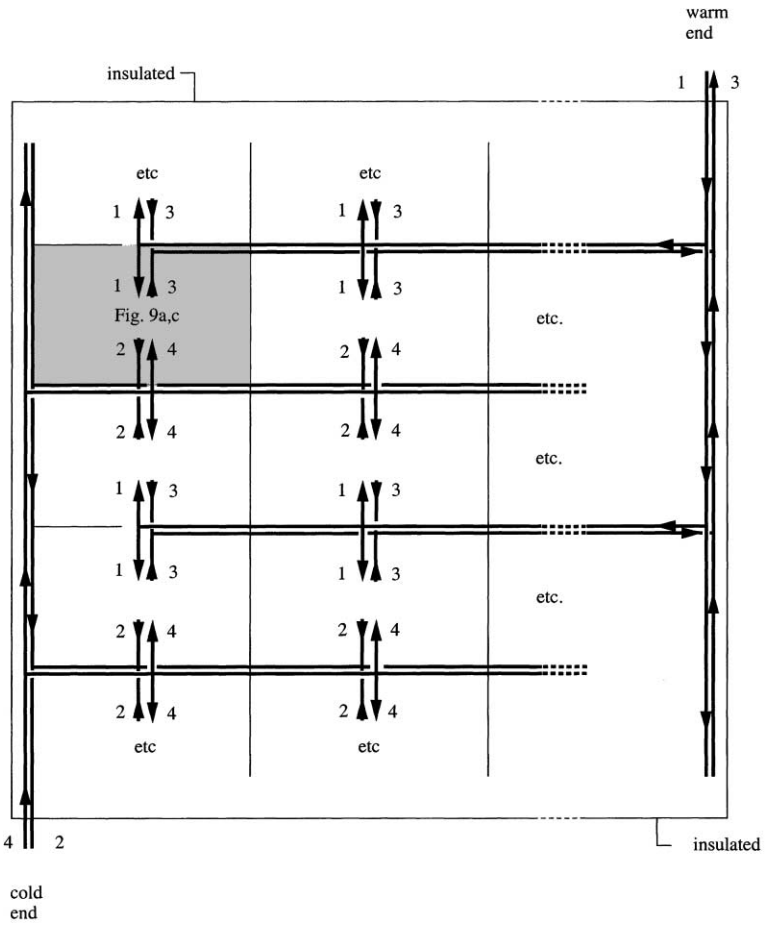

Fig. 10. A larger volume packed with second constructs (Fig. 9a) or third constructs (Fig. 9c), supplied by two intertwining trees, where each tree is a counterflow of two streams.

where $K_h = D_h^2/12$ represents the assumption that fluid friction in the D_h channels is also of the Hagen–Poiseuille type. The centrosymmetry of the flow distribution means that the flow solution must have the form $\dot{m}_1(z) = \dot{m}_2(-z)$ and $P_1(z) = P_2(z)$. Combining Eqs. (5), (8) and (9) we find that

$$P_1 + P_2 = c_1 z + c_2 \tag{10}$$

where $c_1 = \mu \dot{m}_h/(\rho D_h W_0 K_h)$. Next, we combine Eqs. (6)–(8), eliminate P_2 using Eq. (10), and obtain the general solution for $P_1(z)$:

$$P_1 = \frac{c_1}{2} z + \frac{c_2}{z} + c_3 \sinh\left[z\left(\frac{2}{a}\right)^{1/2}\right] + c_4 \times \cosh\left[z\left(\frac{2}{a}\right)^{1/2}\right] \tag{11}$$

where $a = L_0 D_h K_h / K_{0h}$. The general solution for $P_2(z)$ follows from Eq. (10). The centrosymmetry of the two pressure distributions pinpoints two of the constants of integration. To see the centrosymmetry property better, we use the 4-corner pressure notation

$$P_{in} = P_1(L_1/2), \quad P_{2end} = P_2(L_1/2) \tag{12}$$

$$P_{1end} = P_1(-L_1/2), \quad P_{out} = P_2(-L_1/2) \tag{13}$$

Centrosymmetry requires that the average of two diametrically opposed pressures must match the average of the remaining corner pressures,

$$\tfrac{1}{2}(P_{in} + P_{out}) = \tfrac{1}{2}(P_{1end} + P_{2end}) \tag{14}$$

From this condition we obtain $c_2 = P_{in} + P_{out}$. Centrosymmetry also requires that the overall pressure drop along $\dot{m}_1$ channel must be the same as along the $\dot{m}_2$ channel,

$$P_{in} - P_{1end} = P_{2end} - P_{out} \tag{15}$$

which is satisfied if $c_3 = 0$. The remaining constant (c_4) is obtained by substituting Eq. (12) into Eq. (8), and setting $\dot{m}_1 = 0$ at $z = -L_1/2$. The result is

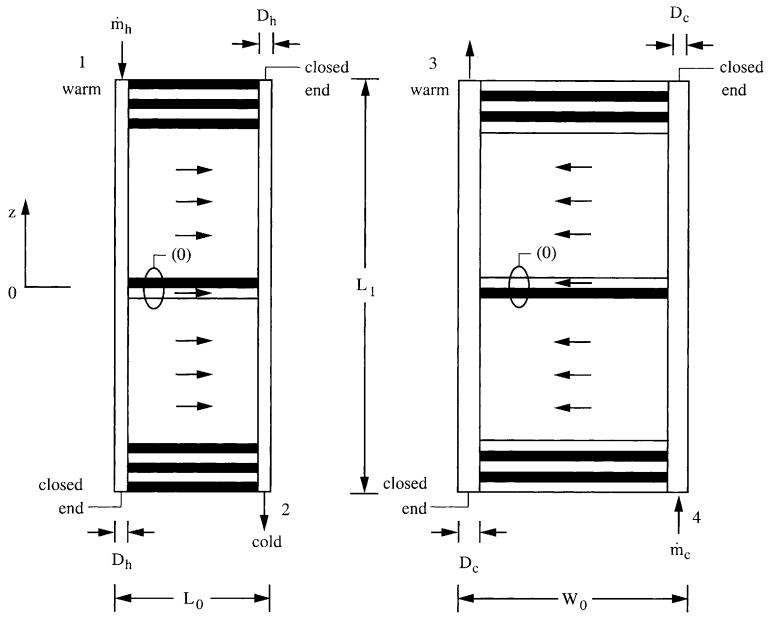

Fig. 11. First construct with unequal flow rates and channel spacings.

$$c_4 = \frac{c_1}{2}\left(\frac{a}{2}\right)^{1/2} \Big/ \sinh\left[\frac{L_1}{2}\left(\frac{2}{a}\right)^{1/2}\right] \tag{16}$$

In conclusion, the resulting flow rate distributions confirms the centrosymmetry property $\dot{m}_1(z) = \dot{m}_2(-z)$,

$$\dot{m}_1 = \frac{1}{2}\dot{m}_h\left(1 + \frac{\sinh[z(2/a)^{1/2}]}{\sinh[(L_1/2)(2/a)^{1/2}]}\right) \tag{17}$$

$$\dot{m}_2 = \frac{1}{2}\dot{m}_h\left(1 - \frac{\sinh[z(2/a)^{1/2}]}{\sinh[(L_1/2)(2/a)^{1/2}]}\right) \tag{18}$$

The nonlinear variation of $\dot{m}_1$ and $\dot{m}_2$ with z means that the flow rate through the core ($\mathrm{d}\dot{m}_1/\mathrm{d}z$) is nonuniform. The flow rate through the top and bottom regions of the core ($z \approx \pm L_1$) is generally larger than through the mid regions ($z \approx 0$). The core flow rate approaches a uniform distribution in the limit where expressions (17) and (18) are linear, namely when $x \ll 1$, where x is defined in Eq. (20). In principle, the flow rate $\mathrm{d}\dot{m}_1/\mathrm{d}z$ could be made uniform by design, by using appropriately tapered side channels ($D_h(z)$) and a nonuniform distribution of microchannel sizes ($K_{0h}(z)$), as suggested in Fig. 4. The expressions for P_1 and P_2 that correspond to Eqs. (17) and (18) allow us to estimate the overall pressure difference across the construct,

$$P_{in} - P_{out} = \frac{\dot{m}_h \mu L_1}{2\rho W D_h K_h}\left(1 + \frac{1}{x\tanh(x)}\right) \tag{19}$$

where x is the dimensionless group

$$x = \frac{L_1}{2}\left(\frac{2}{a}\right)^{1/2} = \left(\frac{L_1^2 K_{0h}}{2LD_h K_h}\right) \tag{20}$$

The overall flow resistance $(P_{in} - P_{out})/\dot{m}_h$ can be minimized by balancing the resistances posed by the D_h channels and the K_{0h} core. To illustrate the opportunity to optimize the geometry, consider the case where x is small in comparison with 1, so that $\tanh(x) \cong x$. In this limit the relationship between global resistance and geometric parameters is

$$\frac{P_{in} - P_{out}}{\dot{m}_h \mu/2\rho} \cong \frac{L_1}{W_0 D_h K_h} + \frac{L_0}{WHK_{0h}} \tag{21}$$

The two terms on the right-hand side account, in order, for the resistances of the vertical D_h channels and the horizontal core flow. When the total space allocated to the construct is fixed ($V_1/W_0 = L_1 L_0 = \text{constant}$, for the path of $\dot{m}_h$) the overall flow resistance (21) is minimal when

$$\frac{L_1}{L_0} = \left(2D_h\frac{K_h}{K_{0h}}\right)^{2/3}\left(\frac{W_0}{V_1}\right)^{1/3} \tag{22}$$

Here V_1 is the volume of the first construct, $V_1 = L_1 L_0 W_0$. The minimized flow resistance that corresponds to this optimal geometry is

$$\left(\frac{P_{in} - P_{out}}{\dot{m}_h/W_0}\right)_{min}\frac{2\rho}{\mu} = \frac{(2^{1/3} + 2^{-2/3})(V_1/W_0)^{1/3}}{(D_h K_h)^{2/3} K_{0h}^{1/3}} \tag{23}$$

The corresponding optimization of the cold flow path 4–3 yields, in place of Eq. (22),

$$\frac{L_1}{W_0}=\left(2D_c\frac{K_c}{K_{0c}}\right)^{2/3}\left(\frac{L_0}{V_1}\right)^{1/3} \tag{24}$$

where $K_c=D_c^2/12$ and $K_{0c}=D_{0c}^2/12$. Eqs. (22) and (24) mean that in an order of magnitude sense

$$\frac{L_1}{L_0}\approx\frac{D_h^2}{D_{0h}^{4/3}}\frac{W_0^{1/3}}{V_1^{1/3}} \tag{25}$$

$$\frac{L_1}{W_0}\approx\frac{D_c^2}{D_{0c}^{4/3}}\frac{L_0^{1/3}}{V_1^{1/3}} \tag{26}$$

By eliminating $L_1V_1^{1/3}$ between Eqs. (25) and (26), we find that

$$\left(\frac{L_0}{W_0}\right)^{1/3}\frac{D_h}{D_c}\left(\frac{D_{0c}}{D_{0h}}\right)^{2/3}=1 \tag{27}$$

This confirms the symmetry assumption made in Fig. 3, namely that when $L_0=W_0$ and $D_{0c}=D_{0h}$, minimal flow resistance requires $D_h=D_c(=D_1)$.

7. Maximum heat transfer rate density

The objective of this paper was to describe the conceptual design of a heat exchanger that takes maximum advantage of the high heat transfer density promised by the use of small-scale channels with laminar flow. The heart of the design are the smallest (elemental) channels, which fill most of the volume allocated to the heat exchanger. Each elemental channel has a length that matches the thermal entrance length of the stream that flows through it. This feature gives the channel the ability to transfer heat at a maximum rate per unit volume.

The rest of the design has the purpose of organizing and connecting the elemental channels so that they fill the heat exchanger volume effectively. The objective is minimum pumping power and maximum thermal contact between hot and cold streams. This leads to a sequence of constructs of increasing size, such that each stream bathes the heat exchanger volume as a tree-shaped flow. Later, the same stream is reconstituted by flowing as a tree, or as a river basin. Each stream has a flow architecture similar to two trees matched canopy to canopy. The two streams, and their associated ramifications, are placed in counterflow at every length scale except the smallest. There, the elemental streams are oriented in crossflow, to facilitate assembly.

The maximum heat transfer rate per unit volume built into this design requires emphasis. It is well known that small channel sizes (D_0) and laminar flow lead to high heat transfer coefficients, $h\approx k/D_0$. This feature is present in the constructal design described in this paper. If the channel is long so that the laminar flow is fully developed, the channel acquires a longitudinal temperature difference associated with the bulk enthalpy increase experienced by the stream. The longitudinal temperature difference, which in the small-scale heat exchanger literature is recognized as an additional "thermal flow" resistance [14], is avoided in the present design.

The thermal-entrance operation of each elemental channel (Fig. 2) offers an additional benefit. If the heat transfer coefficient associated with laminar fully developed flow is h, then according to laminar boundary layer theory the heat transfer coefficient averaged over the entrance (elemental) length is $2h$. In summary, the maximum heat transfer density of the proposed design is due to two effects: the elimination of the longitudinal flow thermal resistances, and the doubling of the heat transfer coefficient that would have been offered by laminar fully developed flow.

The order of magnitude of the heat transfer coefficient in the elemental volumes (k/D_0) justifies the continued push toward miniaturization. Smaller elemental spacings (D_0) lead to greater heat transfer densities. In this direction, the optimization rule described in Section 2 reaches an important limitation. According to Eq. (2), L_0 decreases faster than D_0 because it is proportional to D_0^2. The slenderness ratio L_0/D_0 becomes smaller than the order of 10, or when $(U_0D_0/\nu)Pr<10^2$.

The heart of constructal theory is the generation of flow geometry from the constructal principle: objective fighting against constraints in a malleable (morphing, adapting) flow architecture. Key is the time arrow from small to large, and the realization that the smallest length scale is known and *fixed*. This feature was adopted in recent tree flow models. For this reason, I must stress that constructal theory [1,7–9,13] preceded the tree model proposed by West et al. [15]. The latter proposed a model of an assumed tree of tubes for fluid flow. They acknowledged only three of the assumptions that they made, which I quote: (i) the flow structure is shaped as a tree, (ii) the final branch of the tree is a size-invariant unit, and (iii) the energy required to distribute resources is minimized. These three features were present in constructal theory, but there is an important difference. In constructal theory (i) and (ii) are not assumed. They are deduced from (iii), which is the constructal law reviewed in Section 1.

Acknowledgements

The work reported in this paper was supported by a grant from the National Science Foundation. The author acknowledges with gratitude the comments and

support received on this topic from Profs. S. Lorente, C. Vasile and L.A.O. Rocha.

References

[1] A. Bejan, Shape and Structure, from Engineering to Nature, Cambridge University Press, Cambridge, UK, 2000.
[2] S.J. Kim, S.W. Lee, Air Cooling Technology for Electronic Equipment, CRC Press, Boca Raton, FL, 1995 (Chapter 1).
[3] A.J. Organ, Thermodynamics and Gas Dynamics of the Stirling Cycle Machine, Cambridge University Press, Cambridge, UK, 1992.
[4] G.P. Peterson, A. Ortega, Thermal control of electronic equipment and devices, Adv. Heat Transfer 20 (1990) 181–314.
[5] W. Aung (Ed.), Cooling Technology for Electronic Equipment, Hemisphere, New York, 1988.
[6] J.E. Hesselgreaves, Compact Heat Exchangers: Selection, Design and Operation, Pergamon, Amsterdam, 2001.
[7] A. Bejan, Street network theory of organization in nature, J. Adv. Transport. 30 (1996) 85–107.
[8] A. Bejan, Constructal-theory network of conducting paths for cooling a heat generating volume, Int. J. Heat Mass Transfer 40 (1997) 799–816.
[9] A. Bejan, Advanced Engineering Thermodynamics, second ed., Wiley, New York, 1997 (Chapter 11).
[10] A. Bejan, E. Sciubba, The optimal spacing of parallel plates cooled by forced convection, Int. J. Heat Mass Transfer 35 (1992) 3259–3264.
[11] A. Bejan, Convection Heat Transfer, second ed., Wiley, New York, 1995, p. 126, Fig. 3.16.
[12] S. Weinbaum, L.M. Jiji, A new simplified bioheat equation for the effect of blood flow on local average tissue temperature, J. Biomech. Eng. 107 (1987) 131–139.
[13] A. Bejan, The tree of convective streams: its thermal insulation function and the predicted 3/4-power relation between body heat loss and body size, Int. J. Heat Mass Transfer 44 (2001) 699–704.
[14] A.D. Kraus, A. Bar Cohen, Design and Analysis of Heat Sinks, Wiley, New York, 1995.
[15] G.B. West, J.H. Brown, B.J. Enquist, A general model for the origin of allometric scaling laws in biology, Science 276 (1997) 122–126.